Digital Affine Shear Filter Banks with 2-Layer Structure

Zhihua Che and Xiaosheng Zhuang
Department of Mathematics, City University of Hong Kong, Tat Chee Avenue, Kowloon Tong, Hong Kong
Email: zhihuache2-c@my.cityu.edu.hk, xzhuang7@cityu.edu.hk

***Abstract*—Affine shear tight frames with 2-layer structure are introduced. Characterizations and constructions of smooth affine shear tight frames with 2-layer structure are provided. Digital affine shear banks with 2-layer structure are then constructed. The implementation of digital affine shear transforms using the transition and subdivision operators are given. Numerical experiments on image denoising demonstrate the advantage of our digital affine shear filter banks with 2-layer structure.**

1. Introduction

Directional multiscale representation systems, e.g., dual-tree complex wavelets, curvelets, shearlets, etc., have been shown to be superb over many other multiscale representation systems, such as the tensor-product real-value orthonormal wavelets, in both theory (sparse approximation) and applications, e.g., see [1], [4], [5], [6], [7], [11], [12], [14].

Motivated by the successful applications of affine shear tight frames in [8], [15] and tensor product complex tight framelets for image/video processing in [9], [10], in this paper, we focus on the development and applications of affine shear tight frames with 2-layer structure. The tensor product complex tight framelet filter banks in [9], [10] (TP-$\mathbb{C}$TF$_6$ or TP-$\mathbb{C}$TF$_6^{\downarrow}$) are generated by the tensor product of a 1D filter bank $\{a^+, a^-; b_1^+, b_1^-, b_2^+, b_2^-\}$ having nice frequency splitting property in the sense that a^+, a^- are concentrated on the positive and negative low-frequency part of $[-\pi, \pi)$, respectively, while b_i^+, b_i^- are concentrated on the high-frequency part of positive and negative axis of $[-\pi, \pi)$, respectively for $i = 1, 2$. In such a case, the directional high-pass filters of TP-$\mathbb{C}$TF$_6$ or TP-$\mathbb{C}$TF$_6^{\downarrow}$ have a very nice 2-layer structure. The high-pass filters in the inner layer are 'edge-like' so that they can be used to capture edge-like structure while the high-pass filters in the outer layer are 'oscillating' so that they are suitable for 'texture-like' structure. In this paper, we introduce affine shear tight frames with 2-layer structure that can have arbitrarily number of directional filters in both inner and outer layers.

2. Affine Shear Tight Frames with 2-Layer Structure

Let us first introduce some necessary notation and definitions. We use the following matrices throughout this paper:

$$\mathsf{E} := \begin{bmatrix} 0 & 1 \\ 1 & 0 \end{bmatrix}, \quad \mathsf{S}^\tau := \begin{bmatrix} 1 & \tau \\ 0 & 1 \end{bmatrix}, \quad \mathsf{S}_\tau := \begin{bmatrix} 1 & 0 \\ \tau & 1 \end{bmatrix},$$
$$\mathsf{M}_\lambda := \begin{bmatrix} \lambda^2 & 0 \\ 0 & \lambda^2 \end{bmatrix}, \quad \mathsf{A}_\lambda := \begin{bmatrix} \lambda^2 & 0 \\ 0 & \lambda \end{bmatrix}, \quad \mathsf{D}_\lambda := \begin{bmatrix} 1 & 0 \\ 0 & \lambda \end{bmatrix},$$
$$\mathsf{N}_\lambda := \begin{bmatrix} \lambda^{-2} & 0 \\ 0 & \lambda^{-2} \end{bmatrix}, \quad \mathsf{B}_\lambda := \begin{bmatrix} \lambda^{-2} & 0 \\ 0 & \lambda^{-1} \end{bmatrix},$$

where $\tau \in \mathbb{R}$ and $\lambda > 1$. S^τ and S_τ are the shear operations while $\mathsf{B}_\lambda = \mathsf{A}_\lambda^{-\mathsf{T}}$ is the anisotropic dilation matrix, and $\mathsf{N}_\lambda = \mathsf{M}_\lambda^{-\mathsf{T}}$ is the isotropic dilation matrix. Note that $\mathsf{M}_\lambda = \mathsf{A}_\lambda \mathsf{D}_\lambda$. Define $\mathbb{N}_0 := \mathbb{N} \cup \{0\}$. Let U be a $d \times d$ real-valued invertible matrix. We use the compact notation

$$f_{U;\mathsf{k},\mathsf{n}}(x) := |\det U|^{1/2} f(Ux - \mathsf{k}) e^{-i\mathsf{n}\cdot Ux}, \quad \mathsf{k}, \mathsf{n}, x \in \mathbb{R}^d,$$

for encoding dilation by U, translation by k, and modulation by n. We shall adopt the convention that $f_{U;\mathsf{k}} := f_{U;\mathsf{k},0}$ and $f_{\mathsf{k},\mathsf{n}} := f_{\mathsf{I}_d;\mathsf{k},\mathsf{n}}$ with I_d being the $d \times d$ identity matrix.

An affine shear system is obtained by applying shear, dilation, and translation to generators at different scales. To balance the shear operations, we consider cone-adapted systems, e.g., [5], [7], which usually consists of three subsystems: one subsystem covers the low frequency region, one subsystem covers the horizontal cone $\{\xi = (\xi_1, \xi_2) \in \mathbb{R}^2 : |\xi_2/\xi_1| \le 1\}$, and one subsystem covers the vertical cone $\{\xi = (\xi_1, \xi_2) \in \mathbb{R}^2 : |\xi_1/\xi_2| \le 1\}$ in the frequency plane. Throughout the paper, ξ is used as a one- or two-dimensional variable for the frequency domain with $\xi = (\xi_1, \xi_2)$ if $\xi \in \mathbb{R}^2$. The vertical-cone subsystem could be constructed to be the 'flipped' version of the horizontal-cone subsystem.

Unlike the affine shear systems introduced in [8] that have only a single layer structure, in this paper we introduce affine shear systems with 2-layer structure. That is, at each scale j, the horizontal and vertical cones are further divided into an inner layer and an outer layer. More precisely, Let $\{\varphi\} \cup \Psi_j^{in} \cup \Psi_j^{out}$ to be the set of generators in $L_2(\mathbb{R}^2)$ with

$$\begin{aligned} \Psi_j^{in} &:= \{\psi^{j,\ell,in}(\mathsf{S}^{-\ell}\cdot) : \ell = -r_j^{in}, \dots, r_j^{in}\}, \\ \Psi_j^{out} &:= \{\psi^{j,\ell,out}(\mathsf{S}^{-\ell}\cdot) : \ell = -r_j^{out}, \dots, r_j^{out}\}, \end{aligned} \tag{1}$$

where r_j^{in}, r_j^{out} are nonnegative integers. An *affine shear system with 2-layer structure* (and with the initial scale J)

is then defined to be

$$\begin{aligned}\mathcal{AS}_J(\varphi;\{\Psi_j^{in},\Psi_j^{out}\}_{j=J}^{\infty}) &= \{\varphi_{\mathsf{M}_\lambda^J;\mathsf{k}} : \mathsf{k}\in\mathbb{Z}^2\}\\ &\cup \{h_{\mathsf{A}_{\lambda_j^{in};\mathsf{k}}}, h_{\mathsf{A}_{\lambda_j^{in}\mathsf{E};\mathsf{k}}} : \mathsf{k}\in\mathbb{Z}^2, h\in\Psi_j^{in}\}_{j=J}^{\infty}\\ &\cup \{h_{\mathsf{A}_{\lambda_j^{out};\mathsf{k}}}, h_{\mathsf{A}_{\lambda_j^{out}\mathsf{E};\mathsf{k}}} : \mathsf{k}\in\mathbb{Z}^2, h\in\Psi_j^{out}\}_{j=J}^{\infty}.\end{aligned} \tag{2}$$

In a nutshell, at scale j, the set $\{\varphi_{\mathsf{M}_\lambda^J;\mathsf{k}} : \mathsf{k}\in\mathbb{Z}^2\}$ of functions covers the low-frequency spectrum, $\{h_{\mathsf{A}_{\lambda_j^\iota;\mathsf{k}}}, : \mathsf{k}\in\mathbb{Z}^2, h\in\Psi_j^\iota\} = \{\psi^{j,\ell,\iota}_{\mathsf{S}^{-\ell}\mathsf{A}_{\lambda_j^\iota};\mathsf{k}} : \ell = -r_j^\iota,\dots,r_j^\iota, \mathsf{k}\in\mathbb{Z}^2\}$ covers the horizontal inner cone and outer cone for $\iota = in$ and $\iota = out$, respectively, while the 'flipped' system $\{h_{\mathsf{A}_{\lambda_j^\iota}\mathsf{E};\mathsf{k}}, : \mathsf{k}\in\mathbb{Z}^2, h\in\Psi_j^\iota\} = \{\psi^{j,\ell,\iota}_{\mathsf{S}^{-\ell}\mathsf{A}_{\lambda_j^\iota}\mathsf{E};\mathsf{k}} : \ell = -r_j^\iota,\dots,r_j^\iota, \mathsf{k}\in\mathbb{Z}^2\}$ covers the vertical inner cone and outer cone for $\iota = in$ and $\iota = out$, respectively. See Figure 1 for an illustration.

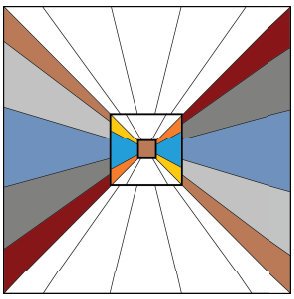

Figure 1. Inner square covered by φ. Inner horizontal cone covered by $\psi^{j,\ell,in}$ (colored area between inner square and middle square, 3 pieces). Outer horizontal cone covered by $\psi^{j,\ell,out}$ (colored area between middle square and outer square, 5 pieces).

We say that $\mathcal{AS}_J(\varphi;\{\Psi_j^{in},\Psi_j^{out}\}_{j=J}^{\infty})$ is an *affine shear tight frame with 2-layer structure* for $L_2(\mathbb{R}^2)$ if all generators $\{\varphi\}\cup\{\Psi_j^{in},\Psi_j^{out}\}_{j=J}^{\infty} \subseteq L_2(\mathbb{R}^2)$ and for all $f\in L_2(\mathbb{R}^2)$,

$$\begin{aligned}\|f\|_2^2 = &\sum_{\mathsf{k}\in\mathbb{Z}^2}\left|\left\langle f,\varphi_{\mathsf{M}_\lambda^J;\mathsf{k}}\right\rangle\right|^2\\ &+\sum_{j=0}^{\infty}\sum_{\iota\in\{in,out\}}\sum_{h\in\Psi_j^\iota}\sum_{\mathsf{k}\in\mathbb{Z}^2}\left|\left\langle f,h_{\mathsf{A}_{\lambda_j^\iota};\mathsf{k}}\right\rangle\right|^2\\ &+\sum_{j=0}^{\infty}\sum_{\iota\in\{in,out\}}\sum_{h\in\Psi_j^\iota}\sum_{\mathsf{k}\in\mathbb{Z}^2}\left|\left\langle f,h_{\mathsf{A}_{\lambda_j^\iota}\mathsf{E};\mathsf{k}}\right\rangle\right|^2.\end{aligned} \tag{3}$$

Similar to [8, Theorem 2], one can give a complete characterization of a sequence of affine shear systems to be a sequence of affine shear tight frames. In this paper, we are interested in the case that all generators are nonnegative in the frequency domain (that is $\widehat{\varphi}\ge 0$ and $\widehat{\psi^{j,\ell,\iota}}\ge 0$ for all j,ℓ,ι), since it leads to simple characterization conditions and easy construction of digital affine shear filter banks. We next detail the construction of such affine shear tight frames with 2-layer structure.

Let $\nu\in C^\infty(\mathbb{R})$ be such that $\nu(x) = 0$ for $x\le -1$, $\nu(x) = 1$ for $x\ge 1$, and $|\nu(x)|^2+|\nu(-x)|^2 = 1$ for all $x\in\mathbb{R}$. Then $\nu\in C^\infty(\mathbb{R})$ is a desired function. Define

$$\boldsymbol{\nu}_{[c,\epsilon]}(\xi) := \begin{cases}\nu(\frac{\xi+c}{\epsilon}) & \text{if } \xi < -c+\epsilon,\\ 1 & \text{if } -c+\epsilon\le\xi\le c-\epsilon,\\ \nu(\frac{-\xi+c}{\epsilon}) & \text{if } \xi > c-\epsilon.\end{cases}$$

The function $\boldsymbol{\nu}_{[c,\epsilon]}$ is a smooth "bump" function supported on $[-c-\epsilon, c+\epsilon]$.

Define $\boldsymbol{\gamma}_\varepsilon = \boldsymbol{\nu}_{[1/2,\varepsilon]}$ for $0<\varepsilon\le 1/2$ and $\boldsymbol{\alpha}_{\lambda,t,\rho} = \boldsymbol{\nu}_{[c,\epsilon]}$ with $c = \lambda^{-2}(1-t/2)\rho\pi$ and $\epsilon = \lambda^{-2}t\rho\pi/2$, where $\lambda>1$, $0<t\le 1$, and $0<\rho\le\frac{1}{1+2\varepsilon}$. Then $\boldsymbol{\alpha}_{\lambda,t,\rho},\boldsymbol{\gamma}_\varepsilon\in C_c^\infty(\mathbb{R})$. In what follows, for simplicity, we shall omit the dependence of $\boldsymbol{\alpha}_{\lambda,t,\rho},\boldsymbol{\gamma}_\varepsilon$ on the parameters and simply write $\boldsymbol{\alpha},\boldsymbol{\gamma}$.

Define $\varphi,\boldsymbol{\omega}_j^{in},\boldsymbol{\omega}_j^{out}$ as follows:

$$\begin{aligned}\widehat{\varphi} &:= \boldsymbol{\alpha}\otimes\boldsymbol{\alpha},\\ \boldsymbol{\omega}_j^{out} &:= \sqrt{|\widehat{\varphi}(\lambda^{-2(j+1)}\cdot)|^2-|\widehat{\varphi}(\lambda^{-2j-1}\cdot)|^2},\\ \boldsymbol{\omega}_j^{in} &:= \sqrt{|\widehat{\varphi}(\lambda^{-2j-1}\cdot)|^2-|\widehat{\varphi}(\lambda^{-2j}\cdot)|^2}.\end{aligned} \tag{4}$$

For $\lambda>1$, define $\ell_\lambda := \lfloor\lambda-(1/2+\varepsilon)\rfloor+1 = \lfloor\lambda+(1/2-\varepsilon)\rfloor$, $\lambda_j^{in} := \lambda^{j-1/2}$, and $\lambda_j^{out} := \lambda^j$. Define for $\xi\ne 0$,

$$\boldsymbol{\Gamma}_j^\iota(\xi) := \sum_{\ell=-r_j^\iota}^{r_j^\iota}\Big(|\boldsymbol{\gamma}(\lambda_j^\iota\frac{\xi_2}{\xi_1}+\ell)|^2+|\boldsymbol{\gamma}(\lambda_j^\iota\frac{\xi_1}{\xi_2}+\ell)|^2\Big),$$

where $r_j^\iota = \ell_{\lambda_j^\iota}$ for $\iota\in\{in,out\}$. One can show that $0<\boldsymbol{\Gamma}_j^\iota\le 2$, $\boldsymbol{\Gamma}_j^\iota(\mathsf{E}\cdot) = \boldsymbol{\Gamma}_j^\iota(\cdot)$, and $\boldsymbol{\Gamma}_j^\iota(t\xi) = \boldsymbol{\Gamma}_j^\iota(\xi)$ for $\xi\ne 0$. Now define $\psi^{j,\ell,\iota}$ for $\iota\in\{in,out\}$ by

$$\widehat{\psi^{j,\ell,\iota}} = \boldsymbol{\omega}_j^\iota((\mathsf{S}_\ell\mathsf{B}_{\lambda_j^\iota})^{-1}\xi)\frac{\boldsymbol{\gamma}(\xi_2/\xi_1)}{\sqrt{\boldsymbol{\Gamma}_j^\iota((\mathsf{S}_\ell\mathsf{B}_{\lambda_j^\iota})^{-1}\xi)}}. \tag{5}$$

We can deduce the following result.

Theorem 1. Let $J\ge J_0\in\mathbb{Z}$ and $\mathcal{AS}_J(\varphi,\{\Psi_j^{in},\Psi_j^{out}\}_{j=J}^{\infty})$ be the affine shear system with 2-layer structure and with $\varphi,\psi^{j,\ell,\iota}$ defined as in (4) and (5). Then for all $J\ge J_0$, $\mathcal{AS}_J(\varphi,\{\Psi_j^{in},\Psi_j^{out}\}_{j=J}^{\infty})$ is an affine shear tight frame with 2-layer structure for $L_2(\mathbb{R}^2)$.

3. Digital Affine Shear Filter Banks with 2-Layer Structure

As proved in [8, Theorem 5], for an affine shear tight frame, it can be subsampled from an affine tight M_λ-framelet, which has a underlying filter bank structure. In this section, we present the construction of the corresponding digital affine shear filter banks with 2-layer structure $\mathcal{DAS}_J(a,\{\mathcal{B}_j^{in},\mathcal{B}_j^{out}\}_{j=0,\dots,J-1})$, where $\{a,\mathcal{B}_j^{in},\mathcal{B}_j^{out}\} = \{a,b_{j,\ell}^\iota,b_{j,\ell}^\iota(\mathsf{E}\cdot),\ell = -r_j^\iota,\dots,r_j^\iota\}_{\iota=in,out;j=0,\dots,J-1}$ is a perfect reconstruction (PR) filter bank at scale j.

We define inner, middle, outer functions $\widehat{a},\widehat{a}_1,\widehat{a}_2\in C(\mathbb{R}^2)$ by

$$\begin{aligned}\widehat{a} &:= \boldsymbol{\nu}_{[c_0,\epsilon_0]}\otimes\boldsymbol{\nu}_{[c_0,\epsilon_0]},\\ \widehat{a}_1 &:= \boldsymbol{\nu}_{[c_1,\epsilon_1]}\otimes\boldsymbol{\nu}_{[c_1,\epsilon_1]},\\ \widehat{a}_2 &:= \boldsymbol{\nu}_{[c_2,\epsilon_2]}\otimes\boldsymbol{\nu}_{[c_2,\epsilon_2]}.\end{aligned} \tag{6}$$

for some parameters $0 < c_0 < c_1 < c_2 = \pi$ and $\epsilon_0, \epsilon_1, \epsilon_2 > 0$ satisfying $c_0 + \epsilon_0 \le \pi/2$ (for downsampling by 2), $(c_1 + \epsilon_1) - (c_0 - \epsilon_0) \le \pi/2$ (for downsampling by 4), and $c_1 - \epsilon_1 - \epsilon_2 \ge \pi/2$ (for downsampling by 4). We identify the function a as a function in $C(\mathbb{T}^2)$ and it will serve as a low-pass filter. The other two are auxiliary functions. One can show that

$$\sum_{\mathsf{k}\in\mathbb{Z}^d} |\widehat{a}_2(\xi + 2\pi\mathsf{k})|^2 = 1, \qquad \xi \in \mathbb{T}^2. \tag{7}$$

In view of (4), we can define the inner and outer functions b^{in}, b^{out} by

$$\begin{aligned} \widehat{b}^{out}(\xi) &:= \sqrt{|\widehat{a}_2(\xi)|^2 - |\widehat{a}_1(\xi)|^2}, \\ \widehat{b}^{in}(\xi) &:= \sqrt{|\widehat{a}_1(\xi)|^2 - |\widehat{a}(\xi)|^2}. \end{aligned} \tag{8}$$

Next, we apply the splitting technique to $\widehat{b}^{\iota}$ for the construction of high-pass filters $b^{j,\ell,\iota}$.

In practice, at scale $j \ge 0$, instead of using 2^j to determine the total number of directions, we use 2^{k_j} for some nonnegative integer. Define

$$\begin{aligned} &\boldsymbol{\gamma}^{k_j,\ell}(\xi) := \boldsymbol{\gamma}_{\varepsilon}(2^{k_j}\xi_2/\xi_1 + \ell), \\ &\boldsymbol{\Gamma}_{k_j}(\xi) := \sum_{\ell=-2^{k_j}}^{2^{k_j}} \left(|\boldsymbol{\gamma}^{k_j,\vec{\ell}}(\xi)|^2 + |\boldsymbol{\gamma}^{k_j,\vec{\ell}}(\mathsf{E}\xi)|^2 \right) \end{aligned} \tag{9}$$

with ε satisfying $0 \le \varepsilon \le \frac{\pi}{c_2+\epsilon_2} - 1/2$ for downsampling purpose. To guarantee smoothness of boundary, we further split $\boldsymbol{\gamma}^{k_j,\ell}(\xi)$ to positive part $\boldsymbol{\gamma}^{k_j,\ell,+}$ and negative part $\boldsymbol{\gamma}^{k_j,\ell,-}$ of ξ_1-axis. Define $\boldsymbol{\gamma}^{k_j,\ell,\pm}(\xi) := \boldsymbol{\gamma}^{k_j,\ell}(\xi)\chi_{\{\pm\xi_1>0\}}$.

Now at scale j, given integers k_j^{in}, k_j^{out} for determining the number of directions, we can obtain functions $\widehat{b}^{\iota}(\xi)\frac{\boldsymbol{\gamma}^{k_j^{\iota},\ell,\pm}(\xi)}{\sqrt{\boldsymbol{\Gamma}_{k_j^{\iota}}(\xi)}}$ concentrating along certain direction in the inner cone and the outer cone for $\iota = in$ and $\iota = out$, respectively. Note that $\widehat{b}^{\iota}(\xi)\frac{\boldsymbol{\gamma}^{k_j^{\iota},\ell,\pm}(\xi)}{\sqrt{\boldsymbol{\Gamma}_{k_j^{\iota}}(\xi)}}$ are not $2\pi\mathbb{Z}^2$-periodic functions. We define $b^{j,\ell,\iota,\pm}$ to be the $2\pi\mathbb{Z}^2$-periodization of $\widehat{b}^{\iota}(\xi)\frac{\boldsymbol{\gamma}^{k_j^{\iota},\ell,\pm}(\xi)}{\sqrt{\boldsymbol{\Gamma}_{k_j^{\iota}}(\xi)}}$ as follows:

$$\widehat{b^{j,\ell,\iota,\pm}}(\xi) := \sum_{\mathsf{k}\in\mathbb{Z}^2} \widehat{b}^{\iota}(\xi + 2\pi\mathsf{k})\frac{\boldsymbol{\gamma}^{k_j^{\iota},\ell,\pm}(\xi + 2\pi\mathsf{k})}{\sqrt{\boldsymbol{\Gamma}_{k_j^{\iota}}(\xi + 2\pi\mathsf{k})}}, \quad \xi \in \mathbb{T}^2.$$

The total number of high-pass filters $b^{j,\ell,\iota,+}$ and $b^{j,\ell,\iota,-}$, $\iota = in, out$, at this scale j is $2(2^{k_j^{in}} + 2^{k_j^{out}} + 2)$.

Given a sequence of nonnegative integers k_j^{ι}, $\iota = in, out; j = 0, \dots, J-1$ for some fixed integer $J \ge 0$ with respect to the finest scale. Let $\mathsf{M} := 2\mathsf{I}_2$, $\mathsf{A}_{j,1}^{\iota} := \mathrm{diag}(4, 2^{k_j^{\iota}})$ and $\mathsf{A}_{j,2}^{\iota} := \mathrm{diag}(2^{k_j^{\iota}}, 4)$. From above, we can obtain a sequence of filter banks:

$$\mathcal{DAS}_J(\{a \downarrow \mathsf{M}, \mathcal{B}_j^{in}, \mathcal{B}_j^{out}\}_{j=0}^{J-1}) \tag{10}$$

with $\mathcal{B}_j^{\iota} := \{b^{j,\ell,\iota,\pm}(\cdot) \downarrow \mathsf{A}_{j,1}^{\iota}, b^{j,\ell,\iota,\pm}(\mathsf{E}\cdot) \downarrow \mathsf{A}_{j,2}^{\iota} : |\ell| \le 2_{k_j^{\iota}}\}$ for $\iota = in, out$ and $j = 0, \dots, J-1$. Here M in $a \downarrow \mathsf{M}$ indicates the downsampling matrix for filtered coefficients with respect to the low-pass filter a and $\mathsf{A}_{j,1}$ indicates downsampling matrix for filtered coefficients with respect to the high-pass filter $b^{j,\ell,\iota,\pm}(\cdot)$, and so on. Now, in view of (7) and (9), we have the following result.

Theorem 2. Retaining notation in this section. Then $\{a \downarrow \mathsf{M}, \mathcal{B}_j^{in}, \mathcal{B}_j^{out}\}$ forms a digital affine shear filter bank with 2-layer structure and with the perfect reconstruction (PR) property:

$$|\widehat{a}(\xi)|^2 + \sum_{\tau,\iota} \sum_{\ell=-2^{k_j^{\iota}}}^{2^{k_j^{\iota}}} \left(|\widehat{b^{j,\ell,\iota,\tau}}(\xi)|^2 + |\widehat{b^{j,\ell,\iota,\tau}}(\mathsf{E}\xi)|^2 \right) = 1,$$

$$\widehat{a}(\xi)\widehat{a}(\xi + 2\pi\omega) = 0, \quad \widehat{b^{j,\ell,\iota,\tau}}(\xi)\widehat{b^{j,\ell,\iota,\tau}}(\xi + 2\pi\omega_1) = 0,$$

for all $\xi \in \mathbb{T}^2$, $|\ell| \le 2^{k_j^{\iota}}$, $\omega \in [\mathsf{M}^{-\mathsf{T}}\mathbb{Z}^2] \cap [0,1)^2 \backslash \{0\}$, and $\omega_1 \in [(\mathsf{A}_{j,1}^{\iota})^{-\mathsf{T}}\mathbb{Z}^2] \cap [0,1)^2 \backslash \{0\}$, where $\iota \in \{in, out\}$ and $\tau \in \{+, -\}$.

4. Digital Affine Shear Transforms

Without loss of generality and for the simplicity of presentation, we shall assume our data live on the dyadic grids $\Lambda(\mathsf{K})$ for $\mathsf{K} := ([0, \dots, 2^{\mathsf{K}_1} - 1] \times [0, \dots, 2^{\mathsf{K}_2} - 1]) \cap \mathbb{N}_0^2$ for $\mathsf{K} = (\mathsf{K}_1, \mathsf{K}_2) \in \mathbb{N}^2$.

For an input data $v : \Lambda(\mathsf{K}) \to \mathbb{C}$, a filter h, and a sampling matrix M, we can define the *transition operator* $\mathcal{T}_{h,\mathsf{M}}v$ and the *subdivision operator* $\mathcal{S}_{h,\mathsf{M}}v$ as in [15]. Using such two operators, for an input data $v^J : \Lambda(\mathsf{K}) \to \mathbb{C}$ and a sequence $\mathcal{DAS}_J(\{a \downarrow \mathsf{M}, \mathcal{B}_j^{in}, \mathcal{B}_j^{out}\}_{j=0}^{J-1})$ of digital affine shear filter banks with 2-layer structure as in (10), the (multilevel) *forward digital affine shear transform* decomposes v^J to a sequence of filtered coefficients

$$\{v^0\} \cup \{w^{j,\ell,\iota,\pm,n} : n = 1, 2, |\ell| \le 2^{k_j^{\iota}}, \iota = in, out;\}_{j=0}^{J-1}, \tag{11}$$

as follows:

$$v^j = \mathcal{T}_{a,\mathsf{M}}v^{j+1} \text{ and } w^{j,\ell,\iota,\pm,n} \quad = \mathcal{T}_{b^{j,\ell,\iota,\pm,n}(\mathsf{E}_n\cdot),\mathsf{A}_{j,n}^{\iota}}v^{j+1}$$

for $|\ell| \le 2^{k_j^{\iota}}, n = 1, 2, \iota = in, out; j = J-1, \dots, 0$, where $\mathsf{E}_1 = \mathsf{I}_2$ and $\mathsf{E}_2 = \mathsf{E}$. $n = 1$ is with respect to the horizontal cone and $n = 2$ is with respect to the vertical cone. The (multilevel) *backward digital affine shear transform* reconstructs a sequence of filtered coefficients in (11) back to a data sequence as follows:

$$\mathring{v}^{j+1} = \mathcal{S}_{a,\mathsf{M}}\mathring{v}^j + \sum_{n,\iota,} \sum_{\ell=-2^{k_j^{\iota}}}^{2^{k_j^{\iota}}} \mathcal{S}_{b^{j,\ell,\iota,\pm,n}(\mathsf{E}_n\cdot),\mathsf{A}_{j,n}^{\iota}} w^{j,\ell,\iota,\pm,n}.$$

for $j = 0, \dots, J-1$ with $\mathring{v}^0 = v$, $n = 1, 2$, $\iota = in, out$.

We next estimate the redundancy rate of our affine shear transforms, which is defined to be the ratio of the size of the output coefficients to the size of the input data. For real-value data v, due to the symmetry of filters, we only need to compute $\{v^0\} \cup \{w^{j,\ell,\iota,+,n} : |\ell| \le 2^{k_j^{\iota}}, n = 1, 2, \iota = in, out\}_{j=0}^{J-1}$. Let $N = 2^{\mathsf{K}_1+\mathsf{K}_2}$ be the size of the input data. At scale j, due to downsampling processing, the coefficient

matrix $w^{j,\ell,\iota,+,1}$ is on the lattice $\Lambda(\widetilde{\mathsf{K}}_1, \widetilde{\mathsf{K}}_2)$, where $\widetilde{\mathsf{K}}_1 = \mathsf{K}_1 - (J-1-j) - k_j^\iota$ and $\widetilde{\mathsf{K}}_2 = \mathsf{K}_2 - (J-j) - 1$, which is of size $\frac{N}{2^{d(J-1-j)}} \cdot \frac{1}{2^{2+k_j^\iota}}$. The total number of high-pass filtered outputs $w^{j,\ell,\iota,+,n}$ at scale j is $2(2^{k_j^\iota+1}+1)$. Consequently, the size of the total output high-pass filtered coefficients at scale j is:

$$\sum_{\iota=in,out} \frac{N}{2^{2(J-1-j)}} \cdot \frac{1}{2^{2+k_j^\iota}} \times 2(2^{k_j^\iota+1}+1) \times 2.$$

The factor '$\times 2$' at the end of the above equation is due to that the outputs $w^{j,\ell,\iota,+,n}$ are complex-valued. The low-pass coefficient v^0 is of size $N/2^{2J}$. Therefore, the redundancy rate r is given by

$$\left(\sum_{\iota} \sum_{j=0}^{J-1} \frac{(2^{-k_j^\iota}+2)}{2^{2j}} + \frac{1}{2^{2J}} \right) \leq \left(\frac{1}{2^{k_{min}+1}} + 1 \right) \frac{16}{3} \leq 8,$$

where $k_{min} := \min\{k_j^{in}, k_j^{out} : j = 0, \ldots, J-1\}$.

Consequently, the redundancy rate of our digital affine shear transforms does not increase with respect to the number of directional filters and it is no more than 8. In fact, the more directional filters we have, the lower redundancy rate of our digital affine shear transforms. For $k_{min} = 0, 1, 2, 3, 4$, the redundancy rate is bounded by $8, \frac{20}{3}, 6, \frac{17}{3}, \frac{11}{2}$, respectively.

Since the implementations forward and backward digital affine shear transforms are based on fast Fourier transforms, one can show that the computational complexity is proportional to $rN \log N$ for N the size of input data and r the redundancy rate of the transform.

5. Numerical Experiments

In this section, we apply our digital affine shear transforms for the tasks of image denoising.

We compare the performance of our systems to several other state-of-the-art directional multiscale representation systems. We use PSNR for performance comparison and the local-soft thresholding technique as given in [8, Section 6]. The parameters in (6) are set as $c_0 = 0.2687\pi, \epsilon_0 = 0.1213\pi, c_1 = 0.5874\pi, \epsilon_1 = 0.05\pi, c_2 = \pi, \epsilon_2 = 0.0274\pi$. We choose $J = 5$; that is, we decompose to 5 scales. The shear parameter $\{(k_4^{in}, k_4^{out}), (k_3^{in}, k_3^{out}), (k_2^{in}, k_2^{out}), (k_1^{in}, k_1^{out}), (k_0^{in}, k_0^{out}))$ is set to be $\{(2,4), (2,4), (1,2), (1,2), (1,1)\})$. The redundancy rate of such a system is about 6.39. The convolution window size L to compute local coefficient variance σ_w is set to be 4, i.e., we are using 9×9 window filter. To avoid boundary effect, we perform symmetric extension for an image with 32 pixels. The results are reported in Table 1.

One can see that for texture-rich images such as `Barbara` and `Fingerprint`, our system outperforms other systems. For relative smooth images such as `Lena`, the performance of our system is comparable to DAS-1 and TP-$\mathbb{C}$TF$_6$ (redundancy rate of $10\frac{2}{3}$), and outperforms other systems.

512×512 Lena							
σ	DAS-2 (6.39)	DAS-1 (6.36)	TP-$\mathbb{C}$TF$_6^{\downarrow}$ (2.67)	TP-$\mathbb{C}$TF$_6$ (10.67)	DT-$\mathbb{C}$WT	DNST	NSCT
5	38.36	38.14(0.22)	38.16(0.2)	38.37(-0.01)	38.25(0.11)	38.01(0.35)	37.71(0.65)
10	35.39	35.12(0.27)	35.22(-0.07)	35.48(-0.09)	35.19(0.2)	35.35(0.04)	34.92(0.47)
30	30.62	30.61(0.01)	30.38(0.11)	30.80(-0.18)	30.50(0.12)	30.68(-0.06)	30.32(0.3)
50	28.30	28.49(-0.19)	28.11(0.27)	28.54(-0.24)	28.22(0.08)	28.21(0.09)	28.02(0.28)
80	26.20	26.54(-0.34)	26.11(0.39)	26.47(-0.27)	26.15(0.05)	25.78(0.42)	25.80(0.4)
100	25.22	25.63(-0.41)	25.21(0.43)	25.52(-0.3)	25.20(0.02)	24.58(0.64)	24.71(0.51)
512×512 Barbara							
σ	DAS-2	DAS-1	TP-$\mathbb{C}$TF$_6^{\downarrow}$	TP-$\mathbb{C}$TF$_6$	DT-$\mathbb{C}$WT	DNST	NSCT
5	37.77	37.32(0.45)	37.63(0.14)	37.84(-0.07)	37.37(0.4)	37.17(0.6)	36.96(0.81)
10	34.14	33.64(0.5)	33.97(0.17)	34.18(-0.04)	33.54(0.6)	33.62(0.52)	33.35(0.79)
30	28.73	28.33(0.4)	28.33(0.4)	28.38(0.35)	27.89(0.84)	27.97(0.76)	27.28(1.45)
50	26.29	26.01(0.28)	25.73(0.56)	25.71(0.58)	25.36(0.93)	25.31(0.98)	24.57(1.72)
80	24.10	23.99(0.11)	23.51(0.59)	23.53(0.57)	23.27(0.83)	22.96(1.14)	22.65(1.45)
100	23.08	23.07(0.01)	22.58(0.5)	22.64(0.44)	22.42(0.66)	22.06(1.02)	21.90(1.18)
512×512 Boat							
σ	DAS-2	DAS-1	TP-$\mathbb{C}$TF$_6^{\downarrow}$	TP-$\mathbb{C}$TF$_6$	DT-$\mathbb{C}$WT	DNST	NSCT
5	36.93	36.63(0.30)	36.74(0.19)	36.92(0.01)	36.73(0.20)	36.04(0.89)	35.79(1.14)
10	33.27	33.01(0.26)	33.10(0.17)	33.41(-0.14)	33.19(0.08)	33.15(0.12)	32.65(0.62)
30	28.25	28.31(-0.06)	27.99(0.26)	28.44(-0.19)	28.23(0.03)	28.44(-0.19)	27.95(0.30)
50	26.08	26.24(-0.16)	25.79(0.29)	26.25(-0.17)	26.06(0.02)	26.23(-0.15)	25.94(0.14)
80	24.23	24.46(-0.23)	24.05(0.19)	24.41(-0.17)	24.22(0.01)	24.17(0.06)	24.11(0.12)
100	23.40	23.67(-0.27)	23.27(0.13)	23.58(-0.18)	23.39(0.00)	23.17(0.22)	23.21(0.18)
512×512 Fingerprint							
σ	DAS-2	DAS-1	TP-$\mathbb{C}$TF$_6^{\downarrow}$	TP-$\mathbb{C}$TF$_6$	DT-$\mathbb{C}$WT	DNST	NSCT
5	36.27	35.20(1.07)	36.29(-0.02)	36.27(0.00)	35.82(0.44)	35.28(0.99)	34.93(1.34)
10	32.08	30.97(1.11)	32.23(-0.15)	32.10(-0.02)	31.74(0.34)	31.76(0.31)	31.33(0.75)
30	26.26	26.24(0.02)	26.37(-0.11)	26.06(0.21)	26.37(-0.11)	26.20(0.07)	26.13(0.13)
50	24.00	24.11(-0.11)	24.01(-0.01)	23.67(0.33)	23.95(0.05)	23.78(0.22)	23.89(0.11)
80	22.10	22.18(-0.08)	21.99(0.11)	21.66(0.44)	21.91(0.19)	21.63(0.47)	21.79(0.31)
100	21.25	21.30(-0.05)	21.09(0.16)	20.75(0.50)	21.01(0.24)	20.56(0.69)	20.77(0.48)

TABLE 1. PSNR of denoised `Lena`, `Barbara`, `Boat`, and `Fingerprint` using different transforms. Numbers in the bracket are the PSNR differences between DAS-2 and the current column. Positive numbers indicate better performance of DAS-2.

Acknowledgments

The research of this work was supported in part by the Research Grants Council of Hong Kong (Project No. CityU 108913) and City University of Hong Kong (Project No.: 7200462 and 7004445).

References

[1] E. J. Candès and D. L. Donoho, New tight frames of curvelets and optimal representations of objects with piecewise C^2 singularities, *Comm. Pure Appl. Math.* **57** (2) (2004) 219–266.

[2] E. J. Candès, L. Demannet, D. Donoho, and L. Ying, Fast discrete curvelet transforms, *Multiscale Model. Simul.* **5** (3) (2006) 861–899.

[3] A. L. Cunha, J. Zhou, and M. N. Do, The nonsubsampled contourlet transform: Theory, design, and applications, *IEEE Trans. Image Proc.*, **15** (10) (2006) 3089–3101.

[4] K. Guo, D. Labate, W. Lim, G. Weiss, and E. Wilson, Wavelets with composite dilations, *Electr. Res. Ann. AMS* **10** (2004) 78–87.

[5] K. Guo, G. Kutyniok, and D. Labate, Sparse multidimensional representations using anisotropic dilation and shear operators, Wavelets and Splines (Athens, GA, 2005), Nashville, TN (2006) 189-201.

[6] K. Guo, D. Labate, W. Lim, G. Weiss, and E. Wilson, Wavelets with composite dilations and their MRA properties, *Appl. Comput. Harmon. Anal.* **20** (2006) 231–249.

[7] K. Guo and D. Labate, Optimal sparse multidimensional representation using shearlets, *SIAM J. Math. Anal.* **9** (2007) 298–318.

[8] B. Han and X. Zhuang, Smooth affine shear tight frames with MRA structures. *Appl. Comput. Harmon. Anal.* **39** (2) (2015) 300–338.

[9] B. Han and Z. Zhao, Tensor product complex tight framelets with increasing directionality, *SIAM J. Imag. Sci.* **7** (2014) 997–1034.

[10] B. Han, Z. Zhao, and X. Zhuang. Directional tensor product complex tight framelets with low redundancy. *Appl. Comput. Harmon. Anal.* **41** (2) (2016) 603–637.

[11] E. J. King, G. Kutyniok, and X. Zhuang, Analysis of data separation and recovery problems using clustered sparsity, *J. Math. Imag. Vis.* 48 (2014), 205–234.

[12] Y.-R. Li, R. H. Chan, L. Shen, Y.-C. Hsu, and W.-Y. I. Tseng, An Adaptive Directional Haar Framelet-Based Reconstruction Algorithm for Parallel Magnetic Resonance Imaging, *SIAM J. Imag. Sci.* **9** (2) (2016) 794–821.

[13] W.-Q. Lim, Nonseparable shearlet transform. *IEEE Trans. Image Proc.* **22** (2013) 2056–2065.

[14] I. W. Selesnick, R. G. Baraniuk, and N. G. Kingsbury, The dual-tree complex wavelet transform, *IEEE Signal Process. Mag.* **22** (6) (2005) 123–151.

[15] X. Zhuang. Digital affine shear transforms: fast realization and applications in image/video processing. *SIAM J. Imag. Sci.* **9** (3) (2016) 1437–1466.